

# RECURSIVE SPARSE LU DECOMPOSITION BASED ON NESTED DISSECTION AND LOW RANK APPROXIMATIONS

XUANRU ZHU AND JUN LAI

**ABSTRACT.** When solving partial differential equations (PDEs) using finite difference or finite element methods, efficient solvers are required for handling large sparse linear systems. In this paper, a recursive sparse LU decomposition for matrices arising from the discretization of linear PDEs is proposed based on the nested dissection and low rank approximations. The matrix is reorganized based on the nested structure of the associated graph. After eliminating the interior vertices at the finest level, dense blocks on the separators are hierarchically sparsified using low rank approximations. To efficiently skeletonize these dense blocks, we split the separators into segments and introduce a hybrid algorithm to extract the low rank structures based on a randomized algorithm and the fast multipole method. The resulting decomposition yields a fast direct solver for sparse matrices, applicable to both symmetric and non-symmetric cases. Under a mild assumption on the compression rate of dense blocks, we prove an  $\mathcal{O}(N)$  complexity for the fast direct solver. Several numerical experiments are provided to verify the effectiveness of the proposed method.

## 1. INTRODUCTION

Consider the following partial differential equations:

$$\begin{cases} \mathcal{L}u = f \text{ in } \Omega, \\ \mathcal{T}u = g \text{ on } \partial\Omega, \end{cases} \quad (1)$$

where  $\mathcal{L}$  is a linear differential operator,  $\mathcal{T}$  is a boundary operator,  $f$  and  $g$  are the source and boundary functions, respectively. The computational domain  $\Omega \in \mathbb{R}^d$  is typically assumed to be simply connected with a Lipschitz continuous boundary. Such kind of PDEs, examples including Laplace and Helmholtz equations with Dirichlet or Neumann boundary conditions [17, 18], commonly arise in many important applications. When equation (1) is solved by finite difference (FD) or finite element method (FEM), it results in a linear system:

$$\mathcal{A}x = b, \quad (2)$$

where matrix  $\mathcal{A}$  is large but sparse. For many applications involving optimizations with PDE constraints, such as optimal design [21] and inverse problems [19], a key challenge is how to solve equation (2) efficiently.

One common approach for solving equation (2) involves iterative methods based on Krylov subspaces, such as Conjugate Gradient (CG) [10] or Generalized Minimal Residual (GMRES) [25], which typically costs near  $\mathcal{O}(N)$  complexity for the matrix-vector product and can complete the iterations in  $\mathcal{O}(1)$  steps when paired with an effective preconditioner. However, the construction of such a preconditioner is often highly nontrivial and many of the existing techniques are problem-specific. A common general-purpose preconditioner is the incomplete LU (ILU) [26], which begins with the classical LU factorization and ignores some of the *fill-ins* below a given threshold. Despite its utility, ILU itself can be computationally expensive, since the number of fill-ins may significantly exceed that of the original sparse matrix. Another well-known approach is the *geometric* multigrid method

---

*Date:* August 27, 2024.

*2020 Mathematics Subject Classification.* 65F05, 65F55, 65N30, 35J05.

*Key words and phrases.* Hierarchical matrices; nested dissection; low rank approximations; fast direct solver.

[13], which is an iterative algorithm based on a sequence of mesh discretizations at multiple scales. It makes use of the smoothing effect of the classical Jacobi or Gauss-Seidel iterations and takes the solution from the coarse grid as the initial guess for the finer grid, leading to rapid convergence for non-oscillatory solutions. However, for equations with oscillatory solutions, such as the Helmholtz and Maxwell equations [17], the convergence rate of multigrid methods tends to deteriorate significantly. In addition, while iterative methods can be very effective for problems with a single right hand side, they become inefficient when multiple right hand sides need to be solved, in which case direct solvers based on the factorization of matrices are highly desirable.

Given the mesh information of PDEs, nested dissection (ND) has emerged as a natural approach for factorizing the matrix from FD or FEM discretization [8]. The basic idea of ND is to recursively partition the graph  $G$  associated with the sparse matrix  $\mathcal{A}$  into two (or more) disjoint subgraphs using a series of separators, continuing this process until each subgraph at the leaf level contains  $\mathcal{O}(1)$  vertices. The method then involves factorizing matrix blocks in a bottom-up manner, starting from the finest level. It is a typical *divide-and-conquer* approach that effectively makes use of the local connectivity properties of the vertices in the FD or FEM graph. However, as the elimination progresses, the system becomes increasingly dense due to the full connectivity of the vertices along the separators. This typically leads to a cost of  $\mathcal{O}(N^{3/2})$  by a straightforward LU decomposition for separators of size  $\mathcal{O}(N^{1/2})$  in two dimensions and  $\mathcal{O}(N^2)$  for separators of size  $\mathcal{O}(N^{2/3})$  in three dimensions [20].

To enhance the efficiency, methods based on low rank approximations have been introduced to accelerate the computation of dense blocks [2], utilizing the structure of *Hierarchical matrix* ( $\mathcal{H}$ -matrix) [14]. These approaches make use of the fact that the underlying Green's functions for the PDEs, while often oscillatory, are smoothly decaying in their amplitudes, leading to far-field interactions that are low rank up to a small tolerance. Examples of  $\mathcal{H}$ -matrices include hierarchically semiseparable (HSS) matrices [4], hierarchical off-diagonal low rank matrices (HODLR) [1],  $H^2$  matrices [15] etc. By hierarchically extracting low rank structures and factorizing them recursively, it could lead to an approximate inverse factorization with asymptotically linear complexity. Due to these advantages, they have been widely used in solving the dense linear systems derived from the discretizations of boundary integral equations [11]. However, when it comes to linear systems from FD or FEM discretizations, the lack of exploitation of unique data structure existed in FD or FEM graphs results in significant overhead in time complexity.

Recently, Cambier et al.[3] proposed a fast factorization algorithm called *spaND*, which stands for *sparsified Nested Dissection*, for the sparse matrices based on nested dissection. This algorithm employs low rank approximations to directly sparsify the separators in the graph without introducing additional fill-ins. Unlike other fast methods for ND that store large blocks in a low rank format, and then compress these dense blocks via fast  $\mathcal{H}$ -algebra, *spaND* sparsifies and eliminates the separators right from the beginning. The algorithm is particularly designed for symmetric positive definite (SPD) matrices and yields a hierarchically sparse  $GG^T$  decomposition with nearly linear complexity. Such decomposition is then used as a preconditioner to construct an efficient iterative solver. *SpaND* fully explores the unique structures in FD or FEM graphs by locally sparsifying dense blocks on the separators. However, it still has certain limitations: it is restricted to symmetric matrices, and the efficiency of low rank structure extraction via QR decomposition is relatively low. Meanwhile, although it is a common strategy to use the sparse factorization as a preconditioner in iterative solvers, it does not fully take the advantages of sparse representation, as compared to the construction of fast direct solver, in the case when multiple right hand sides need to be solved.

Our work builds on the framework of *spaND* with LU decomposition to develop a method called *spaLU*, which stands for sparse LU decomposition. It begins with the nested dissection of a finite

element graph, and recursively sparsifies the dense blocks on the separators through low rank approximations, ultimately resulting in a recursive sparse LU decomposition. Compared to spaND, spaLU offers the following enhancements:

- (1) Based on the sparse LU decomposition, we extend the algorithm from SPD to any invertible sparse matrix  $\mathcal{A}$  derived from FD or FEM discretization without significantly increasing the computational cost.
- (2) We propose a hybrid sampling method from randomized sampling and FMM that accelerates the extraction of low rank structures, providing stable sparsification of dense blocks with a controllable error.
- (3) We present a fast direct solver by utilizing the recursive LU decomposition and demonstrate its linear complexity under a mild assumption on the sparsification rate. It is particularly effective for solving equations with multiple right hand sides.

The paper is organized as follows: Section 2 introduces the notations for nested dissection and provides an overview of recursive sparse LU decomposition. Section 3 details the construction of data structure in nested dissection, focusing on separators and segments. Section 4 proposes an efficient sparsification of segments based on a hybrid interpolative decomposition algorithm, which combines randomized sampling and the field separation idea from FMM. Section 5 presents the complexity analysis of the algorithm. Numerical experiments are provided in Section 6, and the paper is concluded in Section 7.

## 2. PRELIMINARIES

In this section, we introduce the notations and outline the main idea of recursive sparse LU decomposition method. For clarity, we focus on the two dimensional FEM graph, with the extension to three dimensional PDEs to be addressed in future work.

**2.1. Graph and elimination.** Graph structure plays an important role in the computation of sparse matrices [23]. Direct methods such as LU, Cholesky, and QR factorizations can be conveniently illustrated by graphs during the elimination process.

Specifically, a large sparse matrix  $\mathcal{A}$  of order  $n$  corresponds to an undirected graph  $G = (V, E)$  consisted of  $n$  vertices  $V = \{v_i, i = 1, \dots, n\}$  and edges  $E = \{e_{ij}\}$ . An edge  $e_{ij}$  connects vertex  $v_i$  to  $v_j$  if and only if  $\mathcal{A}_{ij}$  is nonzero, making vertex  $v_j$  the adjacent vertex of  $v_i$ . Denote  $\text{Adj}(v_i)$  the set of all adjacent vertices of  $v_i$ , and  $\text{Deg}(v_j)$  the *degree* of a vertex  $v_i$ , which is the number of its adjacent vertices. The adjacent vertices of a vertex set  $V$  are denoted by  $\text{Adj}(V) = \bigcup_{v_i \in V} \text{Adj}(v_i)$ . Generally, the graph associated with a matrix  $\mathcal{A}$  is constructed based on the non-zero elements of  $\mathcal{A}$  [23]. However, for matrix obtained from the discretization of PDEs, the corresponding graph can be constructed easily from the discretization mesh. In particular, the matrix graph for FEM with linear or bilinear elements is identical to the discretization mesh, often referred to as the finite element graph.

When eliminating vertex  $v$  from the graph  $G$  through LU factorization, new non-zero elements, known as *fill-ins*, are generally introduced into the updated matrix. These fill-ins correspond to new edges in the graph. Define the deficiency  $\text{Def}(v)$  as the set of new edges after eliminating  $v$ :

$$\text{Def}(v) = \{e_{ij} \mid v_i, v_j \in \text{Adj}(v), \text{ and } e_{ij} \notin E\}. \quad (3)$$

The new graph after eliminating  $v$  (also referred to as *v-elimination*) is given by

$$G_v = (V_v, E_v) \text{ with } V_v = V \setminus \{v\}, E_v = \{e_{ij} \in E \mid v_i \text{ or } v_j \neq v\} \cup \text{Def}(v). \quad (4)$$

It is evident that different eliminations orders cause fill-ins of different sizes. For example, as shown in Fig. 1, eliminating an arrow-like matrix in Fig. 1a in ascending order (from row 1 to row 4) by LU decomposition results in a large number of fill-ins in the matrix factors  $L$  and  $U$ . In contrast,

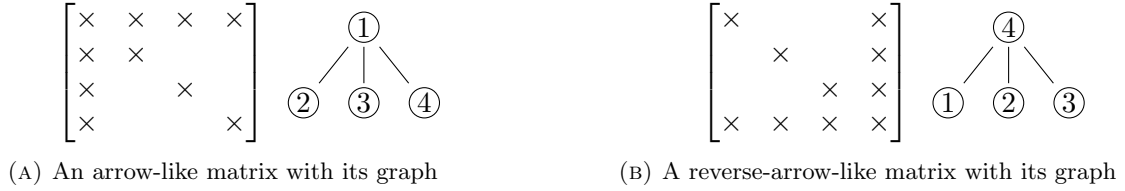


FIGURE 1. A reordering of matrix elements. (a): In the arrow-like matrix, a large number of fill-ins will be introduced in the LU elimination. (b): In the reordered reverse-arrow-like matrix, the LU elimination creates a minimal number of fill-ins.

eliminating the same matrix in the reversed order, as shown in Fig. 1b, results in a minimal number of fill-ins. Therefore, it is crucial to select an elimination order such that the degree of  $\text{Def}(v)$  is minimized after the  $v$ -elimination. However, finding an optimal elimination order of a given matrix is usually NP-complete [7]. One heuristic approach is the *Minimum Degree Ordering* [9], which rearranges the elements in ascending order of their degrees, but in most cases it is still not optimal. Nested dissection offers an approach to address this issue by reordering the vertices to confine the number of fill-ins introduced by elimination to well-separated subgraphs. This approach localizes newly generated edges, with interactions spreading gradually to the entire graph.

**2.2. Nested dissection.** Given the graph  $G$  of a matrix  $\mathcal{A}$ , the nested dissection algorithm [6, 8] partitions the graph  $G = (V, E)$  into three parts: disjoint subgraphs  $G_1 = (V_1, E_1)$ ,  $G_2 = (V_2, E_2)$ , and the *separator*  $S$ , such that

$$\begin{cases} V = V_1 \cup V_2 \cup S, \\ E_1, E_2 \subset E, \\ \{e_{ij} \in E \mid v_i \in V_1, v_j \in V_2\} = \emptyset, \end{cases} \quad (5)$$

as illustrated in Fig. 2a. The algorithm then reorders the rows and columns of  $\mathcal{A}$  so that elements corresponding to  $S$  are placed in the end of matrix  $\mathcal{A}$ , following the blocks associated with  $G_1$  and  $G_2$ , as shown in Fig. 2b. The LU elimination of the two blocks associated with  $G_1$  and  $G_2$  does not affect each other. In addition, subgraphs  $G_1$  and  $G_2$  can be recursively divided in a nested manner until there are  $\mathcal{O}(1)$  vertices in each subgraph at the leaf level. This procedure can be represented by a splitting tree, as illustrated in Fig. 2c.

The factorization procedure for matrix  $\mathcal{A}$  begins by eliminating the elements corresponding to interior vertices in each subgraphs at the leaf level, and then successively eliminating the separators from the finest level to the coarsest. Denote  $A$  as the reordered matrix  $\mathcal{A}$  with nested order  $I$ . The nested dissection algorithm converts equation (2) into

$$Ay = \tilde{b} \quad (6)$$

with

$$A = \mathfrak{J}^\top \mathcal{A} \mathfrak{J}, \quad x = \mathfrak{J}y, \quad \tilde{b} = \mathfrak{J}^\top b, \quad (7)$$

where  $\mathfrak{J}$  is the permutation matrix corresponding to order  $I$ . The algorithm then proceeds by successively eliminating the sub-blocks associated with the subgraphs in the tree structure, from the leaf level to the top level.

An important advantage of nested dissection is both the generation of tree structure and elimination of matrix blocks can be parallellized straightforwardly. However, the effectiveness of nested dissection gradually deteriorates as the elimination progresses to the top of the tree structure. This is because the matrix blocks corresponding to the vertices on the separators become increasingly dense after each elimination. In the end, a dense matrix of order  $\mathcal{O}(N^{1/2})$  needs to be solved, resulting in

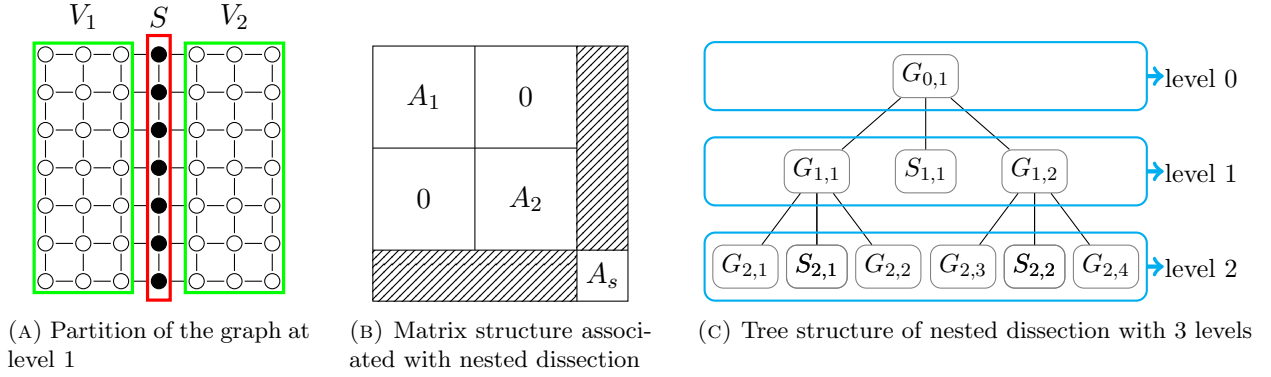


FIGURE 2. An illustration of nested dissection.


 FIGURE 3. Splitting a separator into segments. (a): Separator  $S_i$  is split into 3 segments by the separator  $S_j$ . (b): Segment  $S_i^1$  is split into smaller segments at the lower level.

an  $O(N^{3/2})$  computational complexity. Therefore, to improve the efficiency, an effective solution is required for the dense linear systems on the separators.

**2.3. Sparsification via segments.** As the key to reduce computational complexity is the efficient factorization of dense blocks on the separators, in this section, we outline a novel LU decomposition technique that recursively sparsifies the intermediate dense blocks. This technique enhances overall efficiency by effectively utilizing geometry information of FEM graph throughout the elimination process, particularly by segments introduced in the following.

**2.3.1. Segments.** Motivated by spaND [3], our approach to reduce the complexity of nested dissection focuses on examining the connectivity between different segments. As illustrated in Fig. 3a, during dissection, a separator  $S_i$  is divided into three subsets  $S_i^1 \cup S_i^2 \cup S_i^c$  by  $S_j$ , where  $S_j$  is a separator at the lower level of the tree structure. Similar to how  $S_j$  separates a subgraph of  $G$ ,  $S_j \cup S_i^c$  separates  $S_i$  into two disjoint sets  $S_i^1$  and  $S_i^2$ . We call  $S_i^1$  and  $S_i^2$  the *regular* segments of  $S_i$ , and  $S_i^c$  the *junction* segment. In addition, a regular segment like  $S_i^1$  can be further subdivided into smaller subsets at the subsequent (or lower) level, as shown in Fig. 3b. These descendant segments, like the subgraphs of  $G$ , form a hierarchical tree structure within  $S_i$ .

After eliminating interior vertices at the leaf level, the graph is composed solely of separators, as shown in Fig. 4. We refer to this as the *separator graph*, which is associated with the Schur complement of matrix  $A$  in equation (6). Due to the local connectivity property, where edges can not cross any separator, two segments  $S_i^k$  and  $S_i^l$  from the separator  $S_i$ , as shown in Fig. 4a, are disconnected. Therefore, if we denote by  $A_{k,l}$  the submatrix on the separator graph with row indices  $k$  associated with  $S_i^k$  and column indices  $l$  associated with  $S_i^l$ , then the elements in  $A_{k,l}$  should be all zero. The same sparsity pattern holds for  $A_{l,k}$ . This property can be exploited during the elimination process.

2.3.2. *Sparsification.* In this section, we give a preliminary investigation on the sparsification of the segment  $S_i^k \subset S_i$ , and its neighbor  $V_n$  (i.e., vertex set  $V_n = \text{Adj}(S_i^k)$ ). Let  $V_f$  denote the *far-field* of  $S_i^k$ , where  $V_f = \{v \in V \mid v \text{ disconnects to } S_i^k\}$ . Denote  $A_{i,i}$  the submatrix associated with  $S_i^k$ ,  $A_{i,n}$  and  $A_{n,i}$  the submatrices associated with the interaction between  $S_i^k$  and  $V_n$ , and  $A_{f,n}$  and  $A_{n,f}$  the submatrices associated with the interaction between  $V_n$  and  $V_f$ .

Assume that after applying a suitable permutation  $E_i$ , the Schur complement of  $A$ , denoted by  $A_s$ , can be written as

$$E_i^\top A_s E_i = \begin{bmatrix} A_{i,i} & A_{i,n} \\ A_{n,i} & A_{n,n} & A_{n,f} \\ & A_{f,n} & A_{f,f} \end{bmatrix}. \quad (8)$$

There exists a transformation matrix  $U_{t,i}$ , with details provided in Section 4, that factorizes  $A_{i,n}$  within a tolerance  $\varepsilon$  such that

$$U_{t,i} A_{i,n} = \begin{bmatrix} 0 \\ A_{s,n} \end{bmatrix} + \mathcal{O}(\varepsilon). \quad (9)$$

Similarly, the transformation  $L_{t,i}$  reduces  $A_{n,i}$  to  $[0 \ A_{n,s}]$  up to the same tolerance  $\varepsilon$ . Define the extended transformation matrices as  $U_{T,i} = \begin{bmatrix} U_{t,i} & \\ & I \end{bmatrix}$  and  $L_{T,i} = \begin{bmatrix} L_{t,i} & \\ & I \end{bmatrix}$  with  $I$  the identity matrix such that  $U_{T,i} E_i^\top A E_i L_{T,i}$  is well-defined. Then we have

$$U_{T,i} E_i^\top A E_i L_{T,i} = \begin{bmatrix} A_{r,r} & A_{r,s} & 0 \\ A_{s,r} & A_{s,s} & A_{s,n} \\ 0 & A_{n,s} & A_{n,n} & A_{n,f} \\ & & A_{f,n} & A_{f,f} \end{bmatrix} + \mathcal{O}(\varepsilon). \quad (10)$$

From equation (10), it becomes clear that vertex set  $V_s$ , corresponding to the row indices of  $A_{s,n}$ , remains connected to the neighboring vertices of  $S_i^k$ , that is, the vertex set  $V_n$ . However,  $V_r = S_i^k \setminus V_s$  is no longer connected to  $V_n$ , indicating that  $V_s$  can represent the entire segment  $S_i^k$  in interaction with other segments. Consequently, the corresponding matrix elements of  $V_r$  is decoupled from  $V_n$  (i.e.,  $A_{r,n} = 0$ ,  $A_{n,r} = 0$ ), as illustrated in Fig. 4b. We refer to  $V_s$  as the *skeleton* of  $S_i^k$  and  $V_r$  the *remainder* of  $S_i^k$ . This represents a single step in the sparsification of matrix  $A$ , where the transformations  $U_{T,i}$  and  $L_{T,i}$  eliminate the non-zeros elements associated with remainder  $V_r$  without introducing extra *fill-ins* in the rest of matrix  $A$ . In particular,  $A_{f,f}$ ,  $A_{n,f}$  and  $A_{f,n}$  remain unchanged, so the sparsification is completely local. Once all segments at level  $l$  are sparsified, the corresponding skeletons can be merged to form new segments at the next higher level.

Especially, we combine all the transformations at level  $l$  to form two block-diagonal matrices,  $\mathcal{L}_l$  and  $\mathcal{U}_l$ , with each block corresponding to the sparsification of a single segment. These two matrices have the forms:

$$\mathcal{L}_l = \prod_{i=I_l}^1 L_{T,i,l}^{-1} E_{i,l}^\top, \quad \mathcal{U}_l = \prod_{i=1}^{I_l} E_{i,l} U_{T,i,l}^{-1}, \quad (11)$$

where  $\{1, 2, \dots, I_l\}$  represents all the non-junction segments at level  $l$ ,  $L_{T,i,l}$  and  $U_{T,i,l}$  are the transformation matrices for the  $i$ -th segment, and  $E_{i,l}$  is the permutation matrix for the  $i$ -th segment at level  $l$ . After merging the skeletons, we can recursively apply these transformations to each segment in the higher level. In the end, it results in a decomposition of matrix  $A$ :

$$A \approx \mathcal{U}_L \mathcal{U}_{L-1} \cdots \mathcal{U}_1 \mathcal{L}_1 \cdots \mathcal{L}_{L-1} \mathcal{L}_L. \quad (12)$$

We call the factorization (12) as the recursive sparse LU decomposition, or spaLU, of  $A$ . Further details will be provided in Section 4.



(A) Edge relations for two segments from one separator

(B) Segments after sparsification

FIGURE 4. Sparsification of segments. (a): Two segments  $S_i^l$  and  $S_i^k$  belong to the same separator  $S_i$  but have disjoint edge relations. (b): After the sparsification, the skeleton  $V_s$  of  $S_i^k$  still connects to  $V_n$ , the neighbor of  $S_i^k$ , but its remainder  $V_r$  does not connect to  $V_n$  anymore.

### 3. NESTED STRUCTURE FOR FINITE ELEMENT GRAPH

In this section, we give the details of how to construct the necessary data structures for separators and segments from a finite element graph for use in the recursive LU decomposition.

**3.1. Structure of separators.** For a two dimensional finite element graph, since vertices may not be uniformly distributed, as shown in Figure 5, the key strategy for separating the graph is to identify a polygonal line composed of edges that expands from the graph's center vertex  $c$ . Given a graph  $G = (V, E)$ , we begin by estimating the width and height of the bounding box that contains  $V$ . The center of  $V$ , denoted as  $v_c$ , is determined by calculating the median of the coordinates. The vertex  $c \in V$  closest to  $v_c$  is then selected as the center vertex. The unit vector  $\vec{d}$  along the positive x-axis is chosen as the separating direction if the width of  $V$  is less than the height; otherwise, the positive y-axis is selected as the separating direction.

Define the separator generating function

$$D(u, v, c, \vec{d}) = \frac{\langle u - v, \vec{d} \rangle}{\|u - v\| \|\vec{d}\|} + \theta \frac{\langle u - c, \vec{d} \rangle}{\|u - c\| \|\vec{d}\|}, \quad (13)$$

where  $\langle \cdot, \cdot \rangle$  denotes the inner product in  $\mathbb{R}^2$ . This function  $D(u, v, c, \vec{d})$  provides a degree bias relative to the direction  $\vec{d}$ . The first term in  $D$  measures the alignment of  $u - v$  with  $\vec{d}$ , while the second term, scaled by a parameter  $\theta$  ( $0 < \theta < 1$ ), measures the deviation of the alignment of  $u - c$  from  $\vec{d}$ .

Here we generate the separator by choosing  $u = \text{Next}(v, \vec{d})$  that maximizes  $D(u, v, c, \vec{d})$ . Specifically, we take  $v_0 = c$ ,  $\theta = 0.1$ , and iteratively choose  $v_{i+1} = \text{Next}(v_i, \vec{d})$ ,  $i = 1, \dots, p$ , until  $v_{p+1} = \text{Next}(v_p, \vec{d})$  does not exist in  $V$  or  $D(v_{p+1}, v_p, c, \vec{d}) \leq 0$ . Similarly, vertices  $v_{j-1} = \text{Next}(v_j, -\vec{d})$ ,  $j = -1, \dots, -q$ , are obtained until  $v_{-q-1}$  does not exist in  $V$  or  $D(v_{-q-1}, v_{-q}, c, -\vec{d}) \leq 0$ . The separator  $S$  is then composed of the sequence  $v_{-q}, \dots, v_{-1}, v_0, v_1, \dots, v_p$ , which divides the graph  $G$  into two subgraphs  $G_1$  and  $G_2$  by construction. By recursively applying this procedure, one can identify separators for the subgraphs  $G_1$  and  $G_2$  and their successors, as illustrated in Fig. 5.

**3.2. Structure of segments.** In this section, we provide details on how to obtain segment information. Recall that in Section 2, we denote  $S_{l,i}$  the  $i$ -th separator at level  $l$ . However, this notation is insufficient for constructing the tree structure of segments. To distinguish different segments, particularly their origins and how they divide, we introduce the notation  $S_{l,i}^{j,k}$  to denote the  $k$ -th segment that belongs to the separator  $S_{l,i}$ , and is divided at level  $j$ .

---

**Algorithm 1** Nested dissection in 2D with segment information.

---

**Input:** A set of  $n$  vertices  $V$  with their coordinates, and the associated sparse matrix  $\mathcal{A}$ .

**Output:** Nested dissection order  $I$ , and segment information  $\mathcal{N}$ .

- 1: Extract edge relations  $E$  from the structure of matrix  $\mathcal{A}$  and let the number of layers  $L = \mathcal{O}(\log(N))$ . (Here  $\log$  is logarithm with base 2.)
  - 2: Let  $B$  be the set of boundary segments of  $V$  and  $B = \emptyset$ .
  - 3: Initialize  $I \leftarrow \emptyset$ ,  $l \leftarrow 1$  and  $\mathcal{N} \leftarrow \{\mathcal{N}_1, \dots, \mathcal{N}_L\} = \{\emptyset, \dots, \emptyset\}$
  - 4: **function** NESTED2D( $V, B, l$ )
  - 5:     Find the center vertex  $c$  of  $V$  and the separating direction  $\vec{d}$ .
  - 6:     Set the separator  $S \leftarrow \{c\}$ .
  - 7:     Append vertices from  $V$  to  $S$  by expanding from  $c$  along  $\vec{d}$  and  $-\vec{d}$  using equation (13).
  - 8:     Update  $I \leftarrow I \cup S$ .
  - 9:     Partition  $V$  into two parts  $V_1$  and  $V_2$  by the separator  $S$ .
  - 10:    **for** each boundary segment  $B^k \in B$  **do**
  - 11:       Determine the junction  $S' \leftarrow$  intersection of  $S$  and  $B^k$ .
  - 12:       **if**  $S' \neq \emptyset$  **then**
  - 13:          Split  $B^k$  into  $B_1^k$  and  $B_2^k$ , and replace  $B^k$  by  $B_1^k$  and  $B_2^k$  in  $B$  and  $\mathcal{N}_l$ .
  - 14:       **end if**
  - 15:    **end for**
  - 16:    Set  $B_1 \leftarrow \{B^k \in B \mid B^k \text{ on one side of } S\} \cup \{S\}$
  - 17:    Set  $B_2 \leftarrow \{B^k \in B \mid B^k \text{ on the other side of } S\} \cup \{S\}$ .
  - 18:    Update  $\mathcal{N}_l \leftarrow \{\mathcal{N}_l, S\}$ .
  - 19:    **for**  $i = 1, 2$  **do**
  - 20:       **if**  $l < L$  **then**
  - 21:          NESTED2D( $V_i, B_i, l + 1$ ).
  - 22:       **else**
  - 23:           $I \leftarrow I \cup V_i$ .
  - 24:       **end if**
  - 25:    **end for**
  - 26:    **return**  $I, \mathcal{N}$ .
  - 27: **end function**
- 

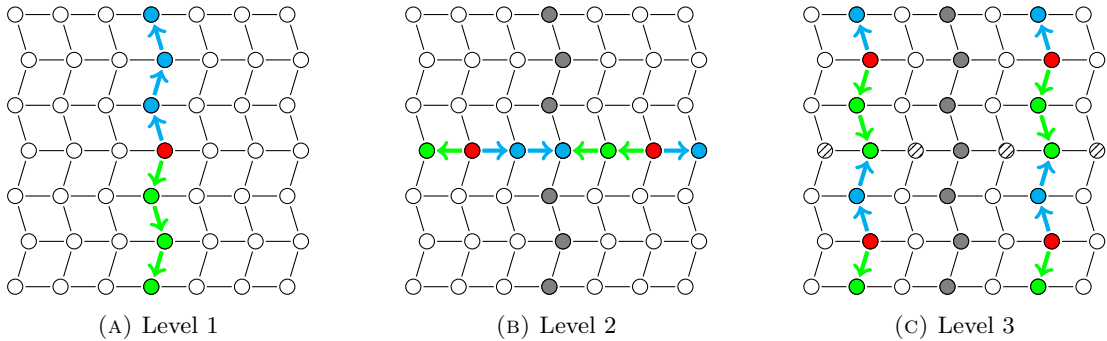


FIGURE 5. A sketch of generating separators. Given the separator direction  $\vec{d}$  in each sub-graph, the separator is generated by expanding from the center vertex (in red) along the direction  $\vec{d}$  (in blue) and  $-\vec{d}$  (in green).

As shown in Fig. 6, suppose that a graph  $G = (V, E)$  is separated into two subgraphs  $G_{1,1}$  and  $G_{1,2}$  by separator  $S_{1,1}$  at level 1, which is denoted as segment  $S_{1,1}^{1,1}$  in our notation. At level 2,



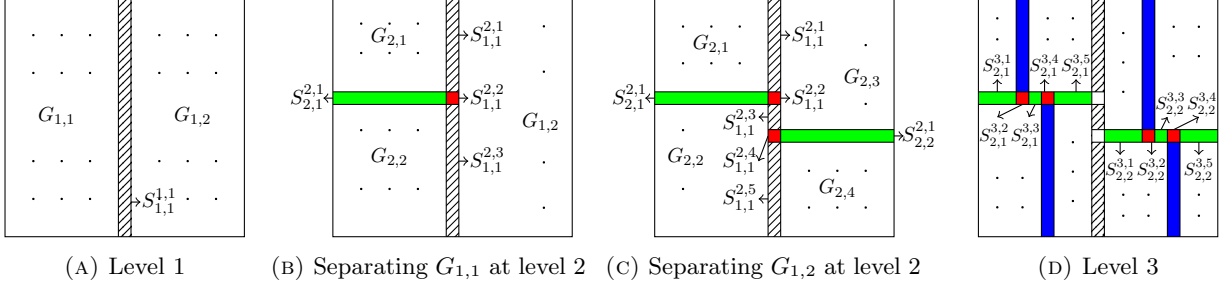


FIGURE 6. Segments obtained from the separators. (a): Separator  $S_{1,1}^{1,1}$  splits the graph into subgraphs  $G_{1,1}$  and  $G_{1,2}$ . (b) and (c): The graph is further separated into 4 subgraphs  $G_{2,1}$ ,  $G_{2,2}$ ,  $G_{2,3}$ ,  $G_{2,4}$ . Meanwhile, separator  $S_{1,1}^{1,1}$  is also split into three regular segments  $S_{1,1}^{2,1}$ ,  $S_{1,1}^{2,3}$ ,  $S_{1,1}^{2,5}$  and two junction segments (in red)  $S_{1,1}^{2,2}$ ,  $S_{1,1}^{2,4}$ , by the new segments  $S_{2,1}^{2,1}$  and  $S_{2,2}^{2,2}$ . (d): Segments  $S_{2,1}^{2,1}$  and  $S_{2,2}^{2,2}$  are further split into finer segments at higher level.

segment  $S_{1,1}^{1,1}$  is further divided into  $S_{1,1}^{2,1} \cup S_{1,1}^{2,2} \cup S_{1,1}^{2,3}$  by the separator  $S_{2,1}$ , or  $S_{2,1}^{2,1}$  by segment notation. Specifically, segment  $S_{2,1}^{2,1}$  divides  $S_{1,1}^{1,1}$  into three segments: two disjoint *regular* segments  $S_{1,1}^{2,1}$  and  $S_{1,1}^{2,3}$ , and one *junction* segment  $S_{1,1}^{2,2}$ . In subgraph  $G_{1,2}$ , the separator  $S_{2,2}$ , also denoted as segment  $S_{2,2}^{2,1}$ , further splits the segment  $S_{1,1}^{2,3}$  into three smaller segments:  $S_{1,1}^{2,3} \cup S_{1,1}^{2,4} \cup S_{1,1}^{2,5}$ . Here, the same notation  $S_{1,1}^{2,3}$  is used to denote one of the smaller segment. At level 3, segment  $S_{2,i}^{2,1}$  is further divided into  $\cup_{k=1}^5 S_{2,i}^{3,k}$  with  $i = 1, 2$ , as shown in Fig. 6d. Following this procedure, all segments can be recursively split into smaller ones, enabling the construction of a tree structure by indexing each segment appropriately.

In the end, the algorithm for partitioning the graph  $G$  by separators with segment information is outlined in Algorithm 1.

#### 4. SPARSIFICATION BASED ON LOW RANK APPROXIMATIONS

In this section, we detail the transformation process mentioned in Section 2, with a specific focus on identifying the low rank structures using *interpolative decomposition* (ID) [5].

**4.1. Interpolative Decomposition.** Given an  $m \times n$  matrix  $B$  with numerical rank  $k$  under the tolerance  $\varepsilon$ , i.e.,  $\sigma_k(B) \geq \varepsilon > \sigma_{k+1}(B)$ , where  $\sigma_k(B)$  is the  $k$ -th singular value of  $B$ , one can apply the strong rank-reveal QR (RRQR) factorization to  $B$  [12]. It yields:

$$B\Pi = Q \begin{bmatrix} R_1 & R_2 \\ & R_\varepsilon \end{bmatrix} = Q \begin{bmatrix} R_1 & R_2 \\ & \mathcal{O}(\varepsilon) \end{bmatrix}, \quad (14)$$

where  $\Pi$  is a permutation matrix, which in most of the time is the same as the permutation generated by column-pivoted QR (CPQR) [10]. Here,  $R_1$  is an upper triangular matrix whose last singular value is greater than  $\mathcal{O}(\varepsilon)$  and  $Q$  is an orthogonal matrix of the form  $[Q_s \quad Q_r]$ , such that:

$$B\Pi = Q_s [R_1 \ R_2] + \mathcal{O}(\varepsilon) = Q_s R_1 [I \ R_1^{-1} R_2] + \mathcal{O}(\varepsilon) = B_s [I \ T] + \mathcal{O}(\varepsilon), \quad (15)$$

where  $T = R_1^{-1} R_2$ ,  $\Pi = [\Pi_s \ \Pi_r]$ ,  $\Pi_s$  represents the first  $k$  columns of  $\Pi$ , and  $B_s = Q_s R_1 = B \Pi_s$  is the *skeleton* of  $B$ . The factorization in the form (15) is called the interpolative decomposition of  $B$  [5], which satisfies:

$$B \underbrace{[\Pi_r \ \Pi_s]}_{L_t} \begin{bmatrix} I \\ -T \\ I \end{bmatrix} = [0 \ B_s] + \mathcal{O}(\varepsilon). \quad (16)$$

The transformation  $U_t$  is generated through a similar procedure when the matrix  $B$  is transposed. Compared to SVD, the interpolative decomposition provides a cost-effective alternative to approximate the low rank structure. Its worst case computational cost is  $\mathcal{O}(mn^2)$ , but typically is  $\mathcal{O}(mnk)$ , which is comparable to the Gram–Schmidt algorithm. Despite this, the computational cost remains significant and reducing it is highly desirable, even if only the constant prefactor in the complexity can be reduced, as it dominates the cost of sparse decomposition.

**4.2. Accelerating the interpolative decomposition.** Note that in the QR factorization (15), we only need the permutation matrix  $\Pi$  and the matrix  $T$  with  $k$  ( $k \ll m$ ) rows. Let  $\Phi$  be an  $h \times m$  matrix, referred to as the *sampling* matrix. By defining  $Y = \Phi B$  and applying RRQR to  $Y$ , we obtain:

$$Y\Pi = Y\Pi_s [I \ T] + \mathcal{O}(\varepsilon), \quad (17)$$

which is

$$\Phi B\Pi = Y\Pi_s [I \ T] + \mathcal{O}(\varepsilon) = \Phi B_s [I \ T] + \mathcal{O}(\varepsilon). \quad (18)$$

If  $\Phi$  is invertible, in which case  $h = m$ , one can verify that

$$B\Pi = B_s [I \ T] + \mathcal{O}(\varepsilon), \quad (19)$$

which has the same form as equation (15). However, in practice, matrix  $\Phi$  is typically of size  $h < m$ . To accelerate the interpolative decomposition, the challenge is to find an efficient method for selecting  $\Phi$ , which we call sampling matrix.

**4.2.1. Randomized Sampling.** There are several methods available to determine the matrix  $\Phi$ . One approach is randomized sampling, which makes use of the properties of random matrices [16]. This method uses a Gaussian random matrix  $G$  as the sampling matrix (i.e.,  $\Phi = G$ ) and then computes the QR factorization of the resulting matrix  $GB$  to efficiently identify the low rank structure of a dense matrix. That is:

$$GB\Pi = QR. \quad (20)$$

The method is simple and elegant. However, it is purely algebraic and does not take into account the underlying geometric information of the matrix. As a result, it may not always be the most optimal choice.

**4.2.2. Sampling by FMM.** The Fast Multipole Method (FMM) [11, 24] is designed to accelerate matrix-vector multiplication in the  $N$ -body interactions by partitioning the interactions into near-field and far-field components. It hierarchically approximate the far-field interaction using low rank structures. FMM is particularly effective for linear elliptic PDEs because the kernels of various integral equations (such as Laplace or Helmholtz) are translation-invariant and decay with increasing distance.

In terms of numerical algebra, consider a sub-matrix  $A_{n,i}$  of  $A$ , where  $A_{n,i}$  represents the edge relations between segment  $S_i^k$  and its neighboring set  $V_n$ , as shown in Fig. 7a. This sub-matrix  $A_{n,i}$  can be compressed via low rank approximation with tolerance  $\varepsilon$ , such that,

$$P^\top A_{n,i} = \begin{bmatrix} A_{\mathcal{N},i} \\ A_{\mathcal{F},i} \end{bmatrix} = \begin{bmatrix} I \\ M_{\mathcal{F},\Gamma} \end{bmatrix} \begin{bmatrix} A_{\mathcal{N},i} \\ Y_{\Gamma,i} \end{bmatrix} + \mathcal{O}(\varepsilon) \quad (21)$$

where  $P^\top$  is a permutation matrix that partitions  $V_n$  into near-field ( $\mathcal{N}$ ) and far-field ( $\mathcal{F}$ ). As illustrated in Fig. 7b,  $\Gamma$  represents the set of indices corresponding to the dashed curve with size  $|\Gamma| < |\mathcal{F}|$ . The edge relations between vertex set  $i$  and the far field  $\mathcal{F}$ , represented by  $A_{\mathcal{F},i}$ , are approximated by the relation between  $i$  and the virtual proxy vertex set  $\Gamma$  represented by  $Y_{\Gamma,i}$  [22]. Therefore, we can take  $\Gamma$  as the sampling matrix. However, the size of  $\Gamma$  highly depends on the distance between the set  $i$  and its far-field vertex set  $\mathcal{F}$ , which increases rapidly if  $\mathcal{F}$  is closely connected to  $i$ .



(A) Edge relation between segment  $S_i^k$  and its neighbor  $V_n$

(B) Far-field  $\mathcal{F}$  is replaced by a proxy curve  $\Gamma$

FIGURE 7. An FMM approach to handling the far-field  $\mathcal{F}$ . (a): The edge relation between segment  $S_i^k$  and its neighboring segments  $V_n$ . (b): The neighbor of  $S_i^k$  is partitioned as  $V_n = \mathcal{N} \cup \mathcal{F}$  where  $\mathcal{N}$  represents the near-field and  $\mathcal{F}$  can be replaced by a proxy curve  $\Gamma$ .

4.2.3. *A hybrid sampling.* In this part, we combine the benefits of randomized sampling and the sampling idea from FMM. Consider a sub-matrix  $A_{n,i}$  with numerical rank  $k$  and let  $P^\top$  be a permutation matrix in the form of (21). Define the sampling matrix  $\Phi$  as

$$\Phi = \begin{bmatrix} I \\ G \end{bmatrix} P^\top, \quad (22)$$

where  $G$  is a Gaussian random matrix of size  $h \times |\mathcal{F}|$ . Based on [16], for  $A_{\mathcal{F},i}$  in (21), there exists an orthonormal matrix  $Q_{\mathcal{F}} \in \mathbb{R}^{|\mathcal{F}|,h}$  with  $h = k + p$  ( $p = 5$  is sufficient in practice) such that

$$A_{\mathcal{F},i} - A_{\mathcal{F},i} Q_{\mathcal{F}} Q_{\mathcal{F}}^\top = \mathcal{O}(\sigma_{k+1}), \quad (23)$$

where  $\sigma_k$  is the  $k$ -th singular value of  $A_{\mathcal{F},i}$  and the QR factorization yields  $(GA_{\mathcal{F},i})^\top = Q_{\mathcal{F}} R_{\mathcal{F}}$ . In other words,  $A_{\mathcal{F},i} \approx A_{\mathcal{F},i} Q_{\mathcal{F}} Q_{\mathcal{F}}^\top = \alpha_{\mathcal{F}} Q_{\mathcal{F}}^\top$ , where  $\alpha_{\mathcal{F}} = A_{\mathcal{F},i} Q_{\mathcal{F}}$ . Therefore,

$$\begin{bmatrix} A_{\mathcal{N},i} \\ A_{\mathcal{F},i} \end{bmatrix} = \begin{bmatrix} I \\ \alpha_{\mathcal{F}} R_{\mathcal{F}}^{-T} \end{bmatrix} \begin{bmatrix} A_{\mathcal{N},i} \\ R_{\mathcal{F}}^\top Q_{\mathcal{F}}^\top \end{bmatrix} + \mathcal{O}(\sigma_{k+1}) = \begin{bmatrix} I \\ \alpha_{\mathcal{F}} R_{\mathcal{F}}^{-T} \end{bmatrix} \begin{bmatrix} A_{\mathcal{N},i} \\ GA_{\mathcal{F},i} \end{bmatrix} + \mathcal{O}(\sigma_{k+1}). \quad (24)$$

As a result, the interpolative decomposition can be applied to the matrix sampled by the sampling matrix (22), denoted by  $Y_{n,i} = \Phi A_{n,i}$ , rather than directly to  $A_{n,i}$ .

Compared to just using randomized sampling given in subsection 4.2.1, this approach requires a smaller Gaussian random matrix. Additionally, there is no need to explicitly compute the proxy mapping  $M_{\mathcal{F},\Gamma}$  as required in the FMM, since random matrix  $G$  effectively replaces the proxy mapping in revealing the rank of interpolative decomposition.

4.3. **SpaLU.** The complete spaLU algorithm to factorize the matrix  $A$  in equation (6) consists of the following steps: elimination of interiors, sparsification, elimination, and merging of the segments.

First, we eliminate interiors for all the subgraphs at the leaf level via straightforward LU factorization, leaving a remainder graph that consists solely of separators. This step yields

$$L_{(L+1)}^{-1} A U_{(L+1)}^{-1} = \begin{bmatrix} I \\ A^{(L)} \end{bmatrix}, \quad (25)$$

where  $A \in \mathbb{C}^{N,N}$ ,  $A^{(L)} \in \mathbb{C}^{N_L, N_L}$ , and  $N_L$  is the number of vertices on the separators. Note that the first  $N - N_L$  rows and columns of  $A$  form a block diagonal matrix and can be factorized in parallel.

Next, we focus on the remaining graph corresponding to the Schur complement  $A^{(L)}$ , as shown in Fig. 8a, which is associated with the separator graph described in subsection 2.3.1. Since it is factorized in a recursive way, let us assume the separators at level  $l + 1$  has been eliminated and

the remaining matrix becomes  $A^{(l)}$ . We then sparsify each segment  $S_{i,j}^{l,k}$  in the rest of the graph via interpolative decomposition, as described in subsection 2.3.2 and illustrated in Fig. 8b, which yields:

$$A_{sp}^{(l)} = U_T^{(l)} A^{(l)} L_T^{(l)} + \mathcal{O}(\varepsilon). \quad (26)$$

Apply LU factorization to the submatrices associated with the sparsified segments as shown in Fig. 8c, and use  $Z_l^{(l)}$  and  $Z_u^{(l)}$  to eliminate the segments  $S_{i,j}^{l,k}$ , as shown in Fig. 8d, which yields

$$Z_l^{(l)} \begin{bmatrix} L_{l,1}^{-1} & & & \\ & L_{l,2}^{-1} & & \\ & & \ddots & \\ & & & \end{bmatrix} A_{sp}^{(l)} \begin{bmatrix} U_{l,1}^{-1} & & & \\ & U_{l,2}^{-1} & & \\ & & \ddots & \\ & & & \end{bmatrix} Z_u^{(l)} = L_{(l)}^{-1} A_{sp}^{(l)} U_{(l)}^{-1} = A_{lu}^{(l)}. \quad (27)$$

Then, we permute the matrix to merge the indices, corresponding to the skeletons after sparsification, into the last of rows and columns, as illustrated in Fig. 8e. This results in:

$$A^{(l-1)} = E_{(l)}^\top A_{lu}^{(l)} E_{(l)} \quad (28)$$

where  $E_{(l)}$  is a permute matrix.

In the end,  $A^{(L)}$  is factorized into

$$WA^{(L)}V \approx I, \quad (29)$$

with

$$W = \prod_{l=1}^L \left( E_{(l)}^\top L_{(l)}^{-1} U_T^{(l)} \right), \quad V = \prod_{l=L}^1 \left( L_T^{(l)} U_{(l)}^{-1} E_{(l)} \right). \quad (30)$$

Therefore, it holds

$$\begin{aligned} A &\approx \tilde{W}^{-1} \tilde{V}^{-1}, \\ \tilde{W} &= \begin{bmatrix} I & \\ & W \end{bmatrix} L_{(L+1)}^{-1}, \\ \tilde{V} &= U_{(L+1)}^{-1} \begin{bmatrix} I & \\ & V \end{bmatrix}. \end{aligned} \quad (31)$$

In the end, we have  $\mathcal{A} = \mathcal{J}\mathcal{A}\mathcal{J}^\top$ . The whole process is summarized in Algorithm 2.

**4.4. Stability Analysis.** In this section, we demonstrate that the spaLU algorithm is stable under certain conditions, both for low rank decomposition and symmetric decomposition.

**4.4.1. Stability of low rank decomposition.** Denote  $E$  the perturbation error for  $A$  after the spaLU decomposition. From equation (12), it is clear that the error introduced by the low rank approximation is:

$$\begin{aligned} \|E\| &= \|A - \mathcal{U}_L \mathcal{U}_{L-1} \cdots \mathcal{U}_1 \mathcal{L}_1 \cdots \mathcal{L}_{L-1} \mathcal{L}_L\| \\ &\leq \prod_{l=1}^L (1 + \|T_{U_l}\|)(1 + \|T_{L_l}\|) \cdot \varepsilon \|A\|, \end{aligned} \quad (32)$$

where  $T_{U_l}$  and  $T_{L_l}$  are matrices of the form  $T$  given in equation (15), associated with  $\mathcal{U}_l$  and  $\mathcal{L}_l$ , respectively. The norm of  $T$  in equation (15) may become uncontrollable if  $R_1$  is highly ill-conditioned. However, Gu and Eisenstat [12, 5] provided a stable algorithm for the RRQR factorization (14), which states:

$$\begin{cases} \sigma_k(R_1) &\geq \frac{1}{\sqrt{1+nk(n-k)}} \sigma_k(B), \\ \sigma_k(R_\varepsilon) &\leq \sqrt{1+nk(n-k)} \sigma_{k+1}(B), \\ \|T\|_F &\leq \sqrt{nk(n-k)}. \end{cases} \quad (33)$$

It implies that  $\|T_{U_l}\| = \mathcal{O}(1)$  and  $\|T_{L_l}\| = \mathcal{O}(1)$ , ensuring stability of the low rank decomposition.

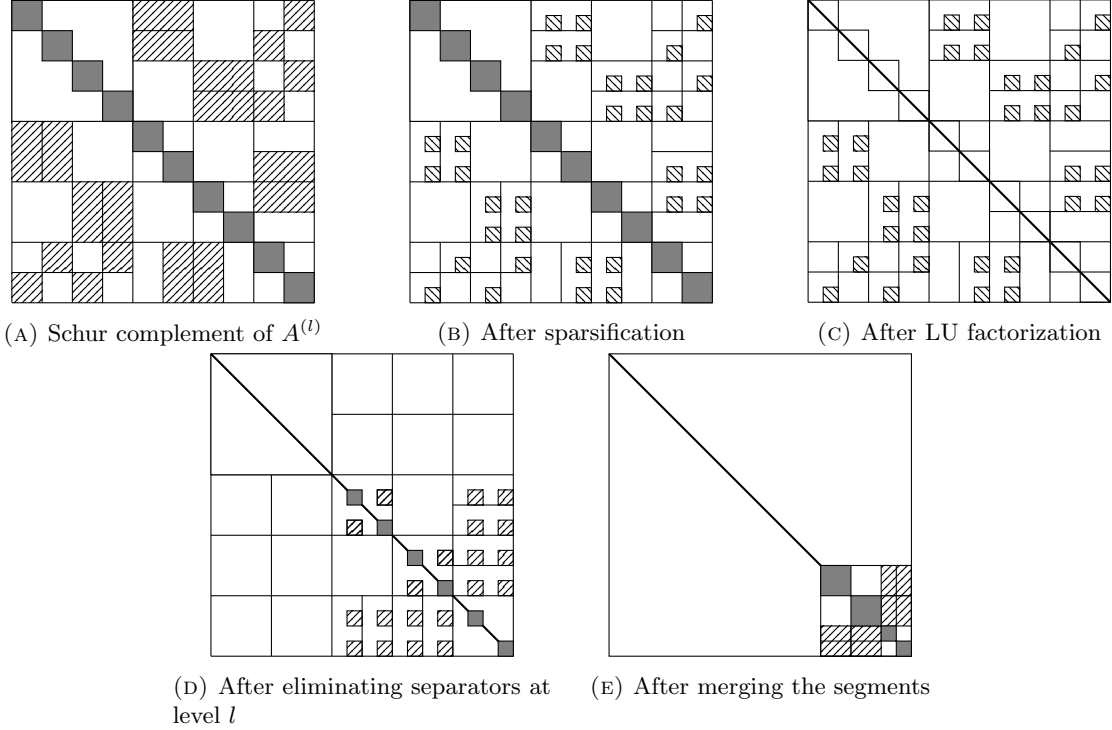


FIGURE 8. An illustration of spaLU in terms of matrix pattern, which begins with the elimination of interior vertices at the leaf level, followed by sparsification, elimination, and merging of segments. Here regions in gray, slashed or back-slashed represent dense sub-matrices and areas in white refer to zero-matrices. Diagonal with thick line denotes identity matrix.

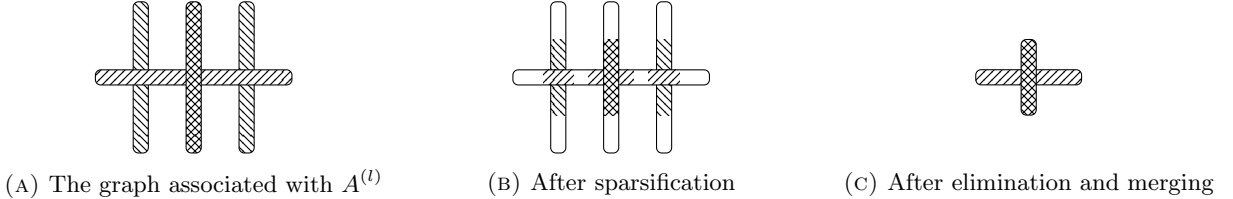


FIGURE 9. An illustration of spaLU in terms of graph, including the sparsification, elimination, and merging of segments. Here regions in backslash line represent segments of level  $l$ , slashed areas corresponds to level  $l - 1$ , and cross region is associated with level  $l - 2$ .

4.4.2. *Stability of symmetric decomposition.* Consider the sub-matrix of  $A$  in the form

$$A_{\text{sub}} = \begin{bmatrix} A_{i,i} & A_{i,n} \\ A_{n,i} & A_{n,n} \end{bmatrix}. \quad (34)$$

If  $A \in \mathbb{C}^{N \times N}$  is symmetric,  $A_{i,n}$  and  $A_{i,n}^*$  share the same interpolative decomposition, allowing the use of  $LDL^T$  instead of LU factorization. Thus, we have  $U_{(l)} = L_{(l)}^*$  for  $l = 0, \dots, L$ , which implies that spaLU preserves symmetry, i.e.,  $\tilde{W} = \tilde{V}^*$ .

Let  $E = A_{\text{sub}} - A_{\text{sub,sp}}$  be the perturbation, where  $A_{\text{sub,sp}}$  is the sparsified matrix. By the Weyl's inequality, for any symmetric matrices  $A$  and  $B$ , it holds  $\lambda_k(A) + \lambda_{\min}(B) \leq \lambda_k(A + B) \leq \lambda_k(A) + \lambda_{\max}(B)$ , where  $\lambda_k(\cdot)$  is the  $k$ -th eigenvalue. Therefore,  $|\lambda_k(A + B) - \lambda_k(A)| \leq \|B\|$ . As a result, if  $\|E\| < \lambda_{\min}(A_{\text{sub}})$ , then  $A_{\text{sub,sp}}$  remains symmetric and stable.

**Algorithm 2** SpaLU factorization algorithm**Input:** Nested ordered matrix  $A$  with segment information  $\mathcal{N}$ , and the tolerance  $\varepsilon$ .**Output:** Factorization term  $L_{(L+1)}, U_{(L+1)}, W, V$ .

---

```

1:  $A^{(L)}, L_{(L+1)}, U_{(L+1)} \leftarrow$  the matrix after eliminating interiors of  $A$ .
2: for level  $l = L, \dots, 1$  do
3:   for each segment  $S_{i,j}^{l,k}$  do
4:      $A^{(l)} \leftarrow$  sparsify  $S_{i,j}^{l,k}$ .
5:   end for
6:   Get  $U_T^{(l)}$  and  $L_T^{(l)}$  through equation (26).
7:   for each segment  $S_{i,j}^{l,k}$  do
8:      $A^{(l)} \leftarrow$  apply LU factorization to  $S_{i,j}^{l,k}$ .
9:   end for
10:  for each segment  $S_{i,j}^{i,k}$  do
11:     $A^{(l)} \leftarrow$  eliminate  $S_{i,j}^{i,k}$ .
12:  end for
13:  Get  $L_{(l)}$ , and  $U_{(l)}$  through equation (27).
14:  Permute  $A^{(l)}$  by merging the sparsified segments, and get  $E_{(l)}$ .
15: end for
16: return  $L_{(L+1)}, U_{(L+1)}, W, V$  where  $W, V$  are defined in equation (30).

```

---

**4.5. A note on factorizing unsymmetric matrices.** Considering the sub-matrix in the form (8) where  $A_{n,i} \neq A_{i,n}$ ,

$$A_{\text{sub}} = \begin{bmatrix} A_{i,i} & A_{i,n} \\ A_{n,i} & A_{n,n} \end{bmatrix}, \quad (35)$$

the current approach to factorize  $A_{\text{sub}}$  is to obtain the sparsification transformations  $U_t$  and  $L_t$  separately, where

$$U_t = \begin{bmatrix} I & -T_2^\top \\ & I \end{bmatrix} \begin{bmatrix} \Pi_{r_2}^\top \\ \Pi_{s_2}^\top \end{bmatrix}, \quad (36)$$

$$L_t = \begin{bmatrix} \Pi_{r_1} & \Pi_{s_1} \end{bmatrix} \begin{bmatrix} I & \\ -T_1 & I \end{bmatrix}.$$

However, using unequal index sets ( $s_1 \neq s_2$ ) often results in a poor condition number for  $A_{i_{s_2}, i_{s_1}}$  (see equation (10)) especially for a large depth level  $L$ , as it breaks the symmetry in the matrix-graph structure. A natural improvement, which is used in this paper, is to apply interpolative decomposition to  $\begin{bmatrix} A_{n,i} \\ A_{i,n}^\top \end{bmatrix}$ , ensuring that  $L_t = U_t^\top$ . Specifically, we have

$$\begin{bmatrix} A_{n,i} \Pi_{r_1} \\ A_{i,n}^\top \Pi_{r_1} \end{bmatrix} = \begin{bmatrix} A_{n,i} \Pi_{s_1} \\ A_{i,n}^\top \Pi_{s_1} \end{bmatrix} T_1 + \mathcal{O}(\varepsilon), \quad (37)$$

which turns out to be much more stable in the computation.

## 5. COMPLEXITY ANALYSIS

**5.1. Complexity of constructing tree structure.** Consider the tree structure with the finest level  $L = \mathcal{O}(\log(N))$  (see Fig. 2c), where the total number of vertices is  $N$ . We assume that the  $i$ th subgraph at level  $l$ , denoted by  $G_{l,i}$ , satisfies following properties:

- (1) Each subgraph  $G_{l,i}$  consists of  $N_l$  vertices with  $N_l = \mathcal{O}(2^{-l}N)$ . In particular, the size of  $G_{L,i}$  at the leaf level is  $\mathcal{O}(1)$ .

- (2) Each subgraph  $G_{l,i}$  attaches to a separator  $S_{l,i}$  of size  $c_l = \mathcal{O}((N_l)^{1/2})$ .
- (3) Each vertex in  $G_{l,i}$  only has  $\mathcal{O}(1)$  edges due to the local connectivity property.

These properties are easily satisfied by the nested structure of finite element graph. In Algorithm 1, the predominant time cost is finding separators, where each step checks  $\mathcal{O}(1)$  neighbors to determine whether the neighbor belongs to  $G_{l,i}$ , and the expansion takes  $c_l$  steps. Hence, the complexity for finding separators via binary search is given by:

$$T_l^{\text{Nd}} = \mathcal{O}\left((N_l)^{1/2} \log(N_l)\right). \quad (38)$$

Therefore, the overall cost for constructing the tree structure of nested dissection is:

$$T^{\text{Nd}} = \sum_{l=1}^L 2^l T_l^{\text{Nd}} = \mathcal{O}\left(\sum_{l=0}^{L-1} 2^l (N_l)^{1/2} \log(N_l)\right) = \mathcal{O}(N). \quad (39)$$

**5.2. Complexity of factorization based on low rank approximations.** To estimate the cost of spaLU during factorization, we need the following sparsity assumption on the low rank structures:

*Sparsity assumption:* let  $e_l$  be the maximum size of segments before sparsification at level  $l$ . The size after sparsification, denoted by  $e'_l$ , satisfies the following property:

$$e'_l \leq q \cdot e_l + \sigma_e, \quad (40)$$

where  $q < 2^{-1/3}$  is the compression rate and  $\sigma_e = \mathcal{O}(1)$  is a positive constant.

**Remark 5.1.** *Since the compression rate  $q$  must be less than 1, our assumption that  $q < 2^{-1/3} \approx 0.8$  is quite mild. It is verified by the numerical experiments in Section 6 for various PDEs, which implies the assumption is also practically reasonable.*

In the elimination of interiors, there are  $2^L$  leaf subgraphs of size  $N_L = \mathcal{O}(1)$ , with neighboring sizes of  $\mathcal{O}(1)$ . Thus, the complexity of eliminating interiors is given by

$$T^{\text{F,int}} = \mathcal{O}(2^L N_L^3) = \mathcal{O}(N). \quad (41)$$

As shown in Fig. 6, separator  $S_{l,i}$  is split into at most  $n_{j,l} = \mathcal{O}\left(2^{\frac{j-l}{2}}\right)$  segments  $S_{l,i}^{j,1}, S_{l,i}^{j,2}, \dots$ , at level  $j$ . This implies that segment  $S_{l,i}^{j,k}$  has size at most

$$s_j = \mathcal{O}\left(\max_{0 \leq l \leq j} \frac{c_l}{n_{j,l}}\right) = \mathcal{O}\left(2^{-j/2} N^{1/2}\right). \quad (42)$$

Consider that there are  $2^l$  separators  $S_{l,1}, S_{l,2}, \dots$  at level  $l$ . The total number of segments  $S_{l,i}^{j,k}$  at level  $j$ , with  $1 \leq l \leq j$ ,  $1 \leq i \leq 2^l$ , and  $1 \leq k \leq n_{j,l}$ , is

$$n_j = \mathcal{O}\left(\sum_{l=1}^j 2^l \cdot n_{j,l}\right) = \mathcal{O}(2^j). \quad (43)$$

Note that every segment is divided into finer regular segments every two levels, as shown in Fig. 6. Conversely, every segment  $S_{l,i}^{j,k}$  at level  $j$  will be merged after two levels of sparsification. In particular, considering  $e_j$  at level  $j$ , since some segments are merged at level  $j-1$ , it holds  $e_{j-1} \leq 2e'_j \leq 2qe_j + 2\sigma_e$ . At level  $j-2$ , a segment  $S_{l,i}^{j-2,k}$  can be merged by some segments  $S_{l,i}^{j-1,p}$  that were not merged at level  $j-1$ , i.e., there exists  $h$  such that  $S_{l,i}^{j-1,p} = S_{l,i}^{j,h}$ , yielding  $e_{j-2} \leq 2qe_j + 2\sigma_e$ . Given  $e_L = N_L \in \mathcal{O}(1)$ , we have:

$$e_{L-2i+1} \leq e_{L-2i} \leq (2q)^i e_L + 2\sigma_e \sum_{j=0}^{i-1} (2q)^j = \mathcal{O}((2q)^i) \quad (44)$$

for  $2 \leq 2i \leq L-1$ , which implies  $e_{L-i} = \mathcal{O}((2q)^{i/2})$  for  $1 \leq i < L$ . Since the QR factorization dominates the computational time during the sparsification, the flops for sparsification at level  $j$  is proportional to

$$T_j^{\text{F,sp}} = \mathcal{O}(e_j^2 e_j') = \mathcal{O}(e_j^3). \quad (45)$$

Therefore, the complexity of total sparsification across all levels is bounded by

$$T^{\text{F,sp}} = \sum_{i=0}^{L-1} T_{L-i}^{\text{F,sp}} = \mathcal{O}\left(\sum_{i=0}^{L-1} 2^{L-i} (2q)^{3i/2}\right) = \mathcal{O}(N). \quad (46)$$

The time complexity of elimination, denoted by  $T^{\text{F,el}}$  can be derived in a manner analogous to  $T^{\text{F,sp}}$ . Hence, the overall cost of spaLU is given by

$$T^{\text{F}} = T^{\text{F,int}} + T^{\text{F,sp}} + T^{\text{F,el}} = \mathcal{O}(N). \quad (47)$$

Furthermore, since solving a triangular matrix equation of size  $n \times n$  costs  $\mathcal{O}(n^2)$ , the time complexity of applying the spaLU factorization as a fast direct solver, derived in a similar way as before, is given by

$$T^{\text{S}} = \mathcal{O}\left(\sum_{i=0}^{L-1} 2^{L-i} (2q)^i\right) = \mathcal{O}(N). \quad (48)$$

## 6. NUMERICAL EXPERIMENTS

In this section, we test the performance of the algorithm by applying it to various PDE problems. All the equations are discretized by FEM using triangular meshes. We test the computational time and residuals with different degrees of freedom (DOF)  $N$  for  $\varepsilon = 10^{-12}, 10^{-10}, 10^{-8}$ , where  $\varepsilon$  is the tolerance defined in Section 4.1. The algorithm is implemented in Matlab and all tests are conducted on a server with 128 GB RAM and an Intel Xeon CPU.

To illustrate the results, we use the following notations in the tables:

- (1)  $T^{\text{Nd}}$  represents the time for constructing nested structure (in seconds).
- (2)  $T^{\text{F}}$  refers to the factorization time via spaLU (in seconds).
- (3)  $T^{\text{S}}$  is the time to apply the factorization to solving the linear system (in seconds).
- (4)  $R_{\text{es}}$  denotes the relative residual  $\|Ax - b\|_2 / \|b\|_2$  after solving equation  $Ax = b$ .
- (5)  $\tilde{q}$  represents the numerical compression factor for segments sparsification, i.e.,  $\tilde{q} = \max_{l=1}^L \frac{e_l'}{e_l}$ , which is used to numerically verify the sparsity assumption  $q$  in equation (40).

**6.1. High-contrast Laplace equation.** Consider the 2D Laplace equation:

$$\begin{cases} \nabla \cdot (a \nabla u) = f, & \Omega = [-1, 1] \times [0, 1], \\ u|_{\partial\Omega} = g(x), \end{cases} \quad (49)$$

where  $f(x) = -4$ ,  $g(x) = x_1^2 + x_2^2 - 1$ , and the variable coefficient  $a(x)$  represents a high-contrast medium characterized by large values of  $\rho$  and small values of  $\rho^{-1}$ , with  $\rho \geq 1$ . We generate  $a$  by smoothing a random field in  $[0, 1]$ , and take  $a = \rho$  when the value of random field is greater than 0.5 and  $a = \rho^{-1}$  otherwise. For  $\rho = 1$ ,  $a$  is simply a constant, while  $\rho = 100$ ,  $a$  becomes highly irregular. Illustrations of the solutions with  $\rho = 1$  and  $\rho = 100$  are provided in Figure 10. One can observe there are significant roughness in the high-contrast medium.

Results for solving the discretized version of equation (49) with  $\varepsilon = 10^{-12}$  are shown in Figure 11. Specifically, Figure 11(a) displays the results for the constant coefficient case  $a = 1$ . The three colored lines correspond to the computational time for constructing the nested dissection structure ( $T^{\text{Nd}}$ ), performing the recursive sparse LU decomposition ( $T^{\text{F}}$ ), and solving the linear system ( $T^{\text{S}}$ ), respectively. Similar results are shown in Figure 11(b) for  $\rho = 100$ . Both results demonstrate that the computational complexity is  $\mathcal{O}(N)$ , which agrees well with our theoretical analysis.



Detailed computational time and accuracy for various value of  $N$  are presented in Table 1. It can be observed that the performance of the solver is not significantly affected by the roughness of  $a$ . In particular, high-contrast medium slightly increases the computational cost and leads to worse residuals due to the larger condition number. One can also see that the numerical sparsity rate  $\tilde{q}$  is only slightly larger for  $\rho = 100$  compared to  $\rho = 1$ , which is expected since the rank of interpolative decomposition increases in high-contrast medium. However,  $\tilde{q}$  is less than 0.8 in all tests, supporting the reasonableness of our sparsity assumption in subsection 5.2. It is also evident that the majority of the computational time is spent on constructing the tree structure for nested dissection ( $T^{\text{Nd}}$ ) and the recursive LU factorization ( $T^{\text{F}}$ ). Once the matrix has been factorized, the amount of time  $T^{\text{S}}$  used to solve the linear system is negligible. This is a key advantage of fast direct solver compared to iterative methods.

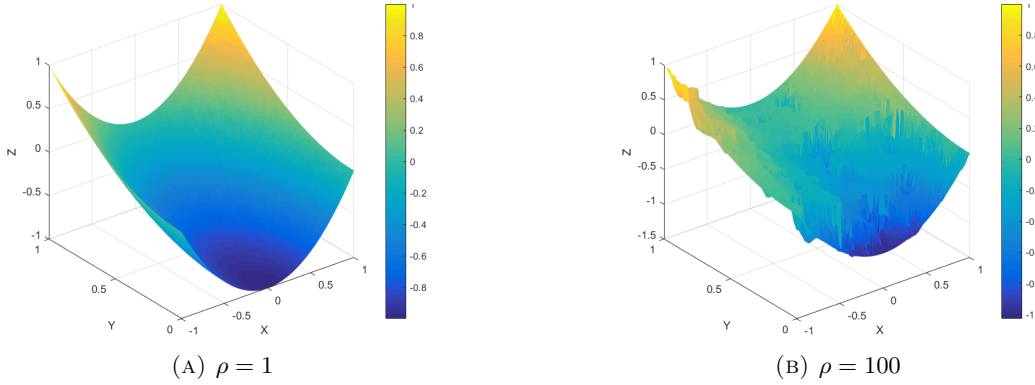


FIGURE 10. Illustrations of solutions for Laplace equations in different media. (a) Constant medium. (b) High-contrast medium.

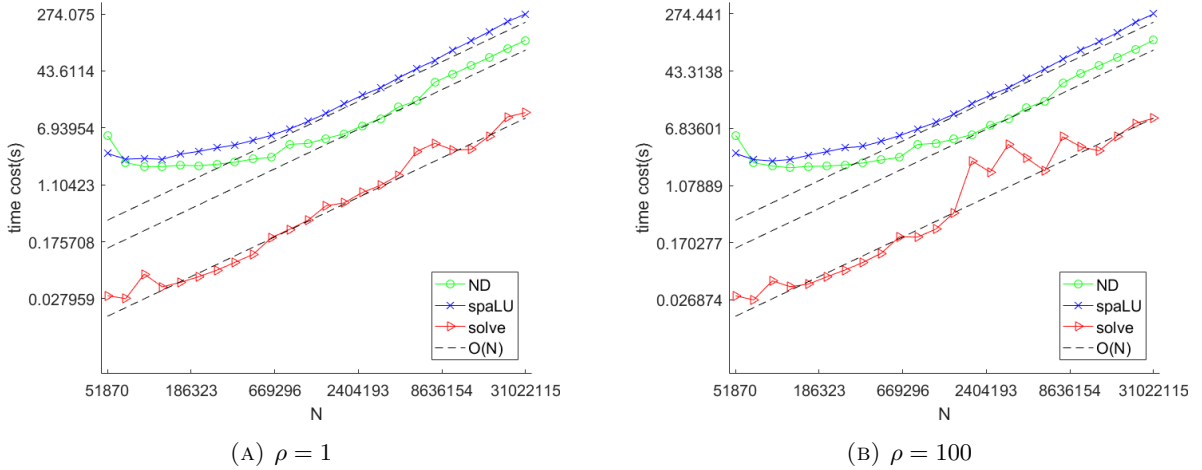


FIGURE 11. Solving the Laplace equation with FEM using spaLU: the computational costs of constructing nested dissection data structure (ND), spaLU, and solving the linear system (solve) align closely with the expected linear complexity  $\mathcal{O}(N)$ , both in the constant medium case (a) and high-contrast medium case (b).

**6.2. Helmholtz equation in a regular domain.** Consider the 2D Helmholtz equation

$$\begin{cases} \Delta u + k^2 u = f, & \Omega = [-1, 1] \times [0, 1], \\ u|_{\partial\Omega} = g(x), \end{cases} \quad (50)$$

$N$	$n \approx N^{1/2}$	$\rho$	$T^{\text{Nd}}$	$T^{\text{F}}$	$T^{\text{S}}$	$\tilde{q}$	$R_{es}$
364 514	604	1	2.29	3.99	0.09	0.63	$6.58 \times 10^{-13}$
		100	2.23	3.82	0.090	0.75	$8.74 \times 10^{-12}$
1 110 389	1054	1	4.18	8.50	0.35	0.66	$3.83 \times 10^{-12}$
		100	4.21	8.30	0.26	0.69	$1.62 \times 10^{-11}$
3 369 978	1836	1	9.37	25.32	1.08	0.67	$1.09 \times 10^{-11}$
		100	9.31	25.26	4.07	0.70	$2.05 \times 10^{-11}$
10 225 605	3198	1	39.41	85.78	3.40	0.65	$9.25 \times 10^{-12}$
		100	40.18	85.97	3.75	0.79	$2.98 \times 10^{-11}$
31 022 115	5570	1	117.11	274.07	11.37	0.66	$1.36 \times 10^{-11}$
		100	117.64	274.44	9.44	0.77	$3.40 \times 10^{-11}$

TABLE 1. The computational time, sparsity rate and residuals for solving 2D Laplace equation using spaLU.

$N$	$n \approx N^{1/2}$	$\varepsilon$	$T^{\text{Nd}}$	$T^{\text{F}}$	$T^{\text{S}}$	$\tilde{q}$	$R_{es}$
364 514	604	$10^{-8}$	2.31	3.87	0.09	0.66	$2.50 \times 10^{-7}$
		$10^{-10}$	2.23	3.79	0.17	0.63	$7.28 \times 10^{-10}$
		$10^{-12}$	2.28	3.92	0.093	0.63	$7.01 \times 10^{-13}$
1 110 389	1054	$10^{-8}$	4.26	8.40	0.40	0.67	$5.61 \times 10^{-7}$
		$10^{-10}$	4.12	8.10	0.47	0.68	$1.16 \times 10^{-9}$
		$10^{-12}$	4.29	8.41	0.81	0.66	$3.95 \times 10^{-12}$
3 369 978	1836	$10^{-8}$	9.04	23.88	0.75	0.68	$8.11 \times 10^{-7}$
		$10^{-10}$	9.17	24.72	1.06	0.67	$1.46 \times 10^{-9}$
		$10^{-12}$	9.03	25.24	1.12	0.67	$1.07 \times 10^{-11}$
10 225 605	3198	$10^{-8}$	39.20	83.14	2.58	0.65	$1.16 \times 10^{-6}$
		$10^{-10}$	38.64	84.52	2.63	0.65	$2.12 \times 10^{-9}$
		$10^{-12}$	39.36	84.66	3.77	0.65	$9.23 \times 10^{-12}$
31 022 115	5570	$10^{-8}$	117.38	273.98	12.56	0.66	$1.49 \times 10^{-6}$
		$10^{-10}$	119.84	277.44	12.89	0.66	$2.68 \times 10^{-9}$
		$10^{-12}$	119.86	276.28	11.60	0.66	$1.35 \times 10^{-11}$

TABLE 2. The computational time, sparsity rate and residuals for solving Helmholtz equation in a regular domain using spaLU.

with  $k = \sqrt{2}$ ,  $f(x) = -1$  and  $g(x) = e^{x_1+x_2}$ . The equation is discretized by FEM with linear elements on a triangular mesh.

Figure 12 shows the computational results for solving the linear system with DOF up to 31 million. It is clear that the computational complexity is on the order of  $\mathcal{O}(N)$  for all three processes, namely, tree structure construction, factorization and solving, which is consistent with our theoretical analysis. The figure also shows that reducing the tolerance only slightly decreases the computational cost. The reason is due to the rapid decay of singular values of the submatrices associated with segments, leading to a relatively stable size of skeletons even with smaller tolerance. More detailed results are provided in Table 2. One can see the sparsity rate  $\tilde{q}$  is almost constant (around 0.6) across different DOF and tolerance levels, implying that it may be an intrinsic property related to the PDE itself. The residual  $R_{es}$  closely matches the compression tolerance  $\varepsilon$ , with an average loss of one digit, indicating the algorithm is very stable. Furthermore, the time required to apply the factorization for solving the linear system is significantly less than the time needed for the factorization process itself, as observed in the previous example. This efficiency suggests that our solver is highly effective when multiple right hand sides need to be solved.

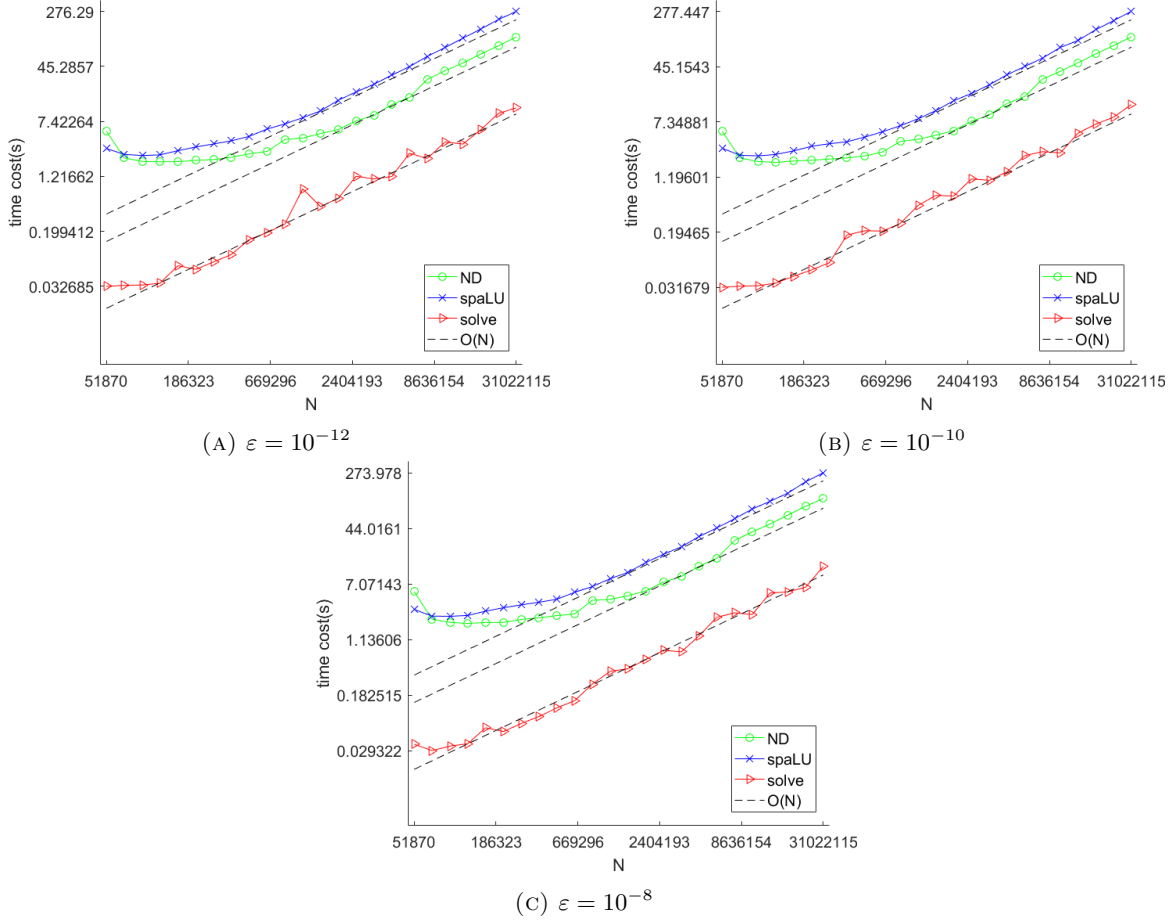


FIGURE 12. Solving the discretized Helmholtz equation with up to 31 million unknowns via spaLU. The computational time for nested dissection tree (ND), factorization (spaLU), and solving the linear systems based on the factorization (solve) are plotted. The black dashed line indicates the computational complexity of all the three processes is on the order of  $\mathcal{O}(N)$ .

**6.3. Helmholtz equation in an irregular domain.** Consider the 2D Helmholtz equation within an irregular domain  $\Omega$ :

$$\begin{cases} \Delta u + k^2 u = f(x), & \text{for } x \in \Omega, \\ u|_{\partial\Omega} = g(x), \end{cases} \quad (51)$$

where  $k = \sqrt{2}$ ,  $f(x) = -1$ ,  $g(x) = e^{x_1+x_2}$ , and  $\Omega$  is a polygonal domain, as shown in Fig. 13(a). The figure also shows the structure of nested partition. Computational results for  $\varepsilon = 10^{-12}$  are shown in Fig. 13(b). Once again, we can see that all the three processes, including the tree structure construction, recursive sparse LU decomposition and applying the factorization for solving linear system, are all on the order of  $\mathcal{O}(N)$ . Compared to the regular domain, the compression rate  $\tilde{q}$  slightly increases, but is still less than 0.8 and satisfies our sparsity assumption. In terms of efficiency, the factorization time in the irregular domain is roughly 0.106 million DOF per second, compared to approximately 0.112 million DOF per second in the regular domain. The difference is minor, which implies the solver is efficient in the irregular domain as well.

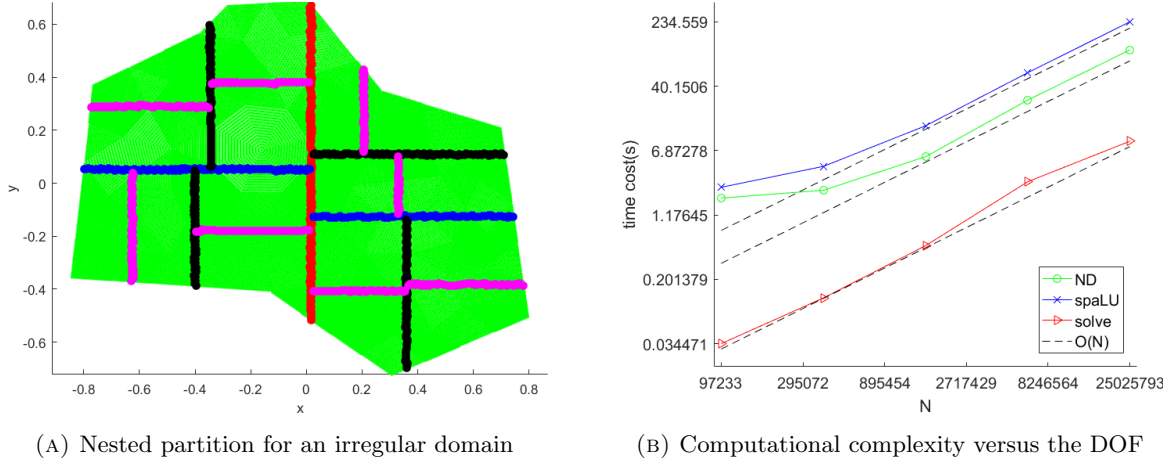


FIGURE 13. Solving the discretized Helmholtz equation in an irregular domain via spaLU. The computational time for nested dissection tree (ND), factorization (spaLU), and solving the linear systems based on the factorization (solve) are plotted. The black dashed line indicates the computational complexity of all the three processes is on the order of  $\mathcal{O}(N)$ .

$N$	$n \approx N^{1/2}$	$T^{\text{Nd}}$	$T^{\text{F}}$	$T^{\text{S}}$	$\tilde{q}$	$R_{es}$
97233	312	1.86	2.50	0.03	0.72	$6.32 \times 10^{-13}$
390049	625	2.31	4.45	0.12	0.55	$8.37 \times 10^{-13}$
1562433	1250	5.81	13.55	0.51	0.76	$9.20 \times 10^{-13}$
6254209	2501	27.36	58.06	2.92	0.78	$1.43 \times 10^{-12}$
25025793	5003	108.53	234.55	8.86	0.79	$1.82 \times 10^{-12}$

TABLE 3. The computational time, sparsity rate and residuals for solving Helmholtz equation in a irregular domain using spaLU.

**6.4. Laplace equation with anisotropic coefficient.** Consider the 2D Laplace equation in anisotropic medium

$$\begin{cases} \nabla \cdot (D \nabla u(x)) = f, & \Omega = [-1, 1] \times [0, 1], \\ u|_{\Gamma_1} = g(x), \\ \frac{\partial u}{\partial n}|_{\Gamma_2} = h(x), \end{cases} \quad (52)$$

where  $f(x) = -4$ ,  $g(x) = x_1^2 + x_2^2 - 1$  and  $h(x) = 2x_2$ , with  $\Gamma_2 = \{(x_1, x_2) \mid -1 < x_1 < 1, x_2 = 1\}$  and  $\Gamma_1 = \partial\Omega \setminus \Gamma_2$ . The coefficient  $D = \begin{bmatrix} 1 & 1 \\ 0 & 1 \end{bmatrix}$  is an asymmetric matrix, representing the anisotropic medium. The resulting stiffness matrix  $\mathcal{A}$  from FEM is unsymmetric in this case.

Numerical results for numerically solving equation (52) with up to 31 million DOF via spaLU are shown in Fig. 14. Considering that Cholesky factorization for symmetric matrices generally requires about half the complexity of LU factorization for unsymmetric matrices of the same size, the factorization for an unsymmetric matrix typically takes twice as long as compared to the same sized symmetric matrix. However, our numerical experiments show that for unsymmetric matrices, spaLU is significantly faster than twice the time required of symmetric matrices. In particular, compared to the computational time for isotropic case in Example 1, where symmetric matrices are factorized, the factorization time for the anisotropic case only increases by roughly 30 percent for the same amount of DOF. It implies the proposed sampling method considerably accelerate the interpolative decomposition for unsymmetric matrices. Meanwhile, the method still follows the rule

of linear complexity in the unsymmetric case, with the sparsity rate  $\tilde{q}$  is consistently less than 0.8, thus satisfying our sparsity assumption.

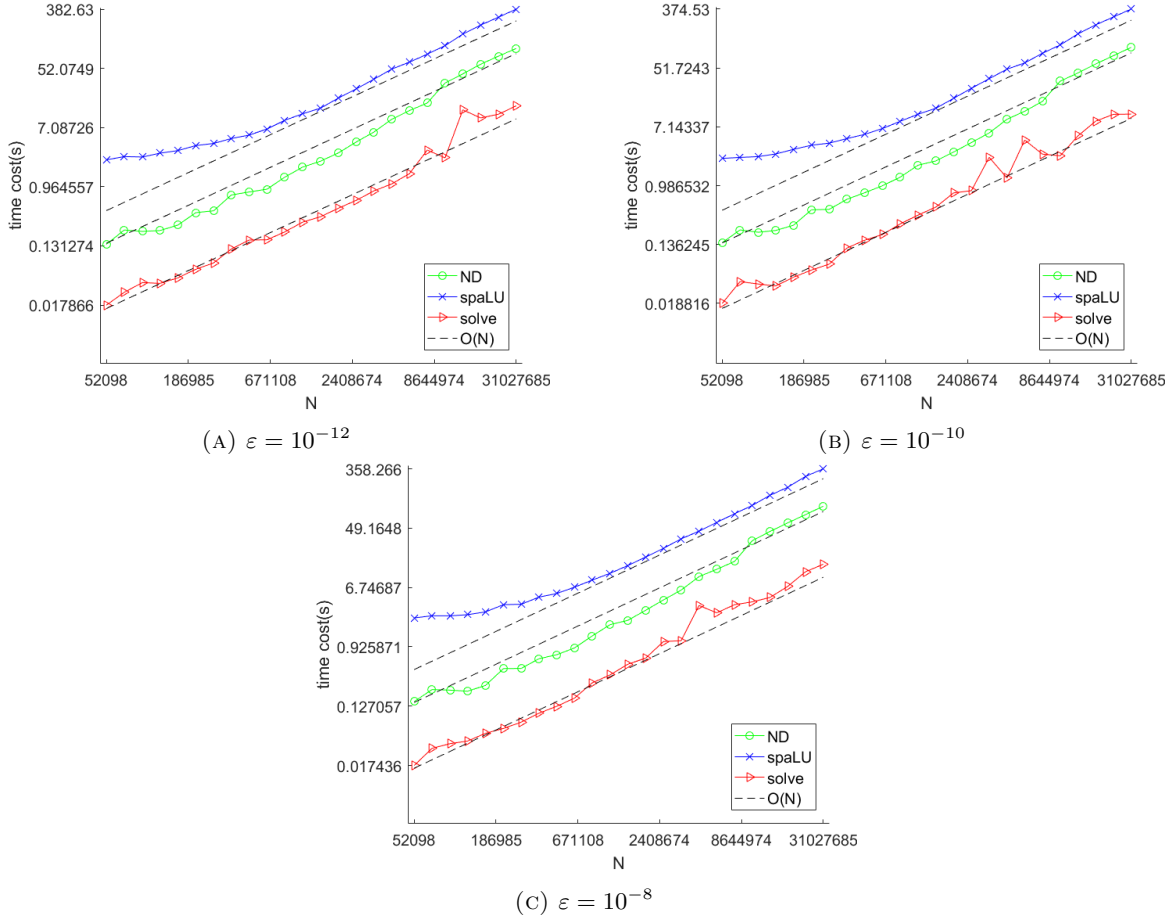


FIGURE 14. Solving the discretized anisotropic Laplace equation via spaLU. The computational time for constructing nested dissection tree (ND), factorization (spaLU), and solving the linear systems based on the factorization (solve) are plotted. The black dashed line indicates the computational complexity of all the three processes is on the order of  $\mathcal{O}(N)$ .

## 7. CONCLUSION

In this paper, we have demonstrated an efficient approach for solving large sparse linear systems resulting from the FD or FEM discretization of PDEs, based on the proposed recursive sparse LU decomposition. By employing nested dissection and low rank approximations, we reorganized the matrix structure and successfully implemented a hierarchical sparsification of dense blocks on the separators. Our hybrid sampling algorithm, which combines ideas from randomized sampling and the FMM, effectively skeletonized the dense blocks, enabling the construction of a fast direct solver applicable to both symmetric and unsymmetric matrices. The theoretical complexity of the solver is  $\mathcal{O}(N)$  under a mild compression rate assumption, which has been confirmed by the numerical experiments. Potential applications of the solver include large-scale optimization problems with PDE constraint or inverse problems, where a large number of forward solves are required. Extension of the algorithm to three dimensional PDEs is currently under investigation.

$N$	$n \approx N^{1/2}$	$\varepsilon$	$T^{\text{Nd}}$	$T^{\text{F}}$	$T^{\text{S}}$	$\tilde{q}$	$R_{es}$
365 118	604	$10^{-8}$	0.62	4.88	0.10	0.73	$5.96 \times 10^{-7}$
		$10^{-10}$	0.62	4.80	0.12	0.57	$2.02 \times 10^{-10}$
		$10^{-12}$	0.73	4.89	0.12	0.69	$1.02 \times 10^{-12}$
1 111 443	1054	$10^{-8}$	1.94	10.85	0.36	0.76	$1.16 \times 10^{-6}$
		$10^{-10}$	1.96	10.91	0.37	0.60	$2.32 \times 10^{-10}$
		$10^{-12}$	1.87	11.28	0.29	0.74	$2.80 \times 10^{-12}$
3 371 814	1836	$10^{-8}$	6.19	34.33	1.14	0.73	$1.54 \times 10^{-6}$
		$10^{-10}$	5.81	35.96	2.56	0.62	$3.76 \times 10^{-10}$
		$10^{-12}$	6.09	36.08	0.84	0.73	$4.10 \times 10^{-11}$
10 228 803	3198	$10^{-8}$	32.24	105.15	4.16	0.69	$1.01 \times 10^{-6}$
		$10^{-10}$	33.13	111.92	2.70	0.61	$4.57 \times 10^{-10}$
		$10^{-12}$	31.74	111.85	2.56	0.68	$2.89 \times 10^{-12}$
31 027 685	5570	$10^{-8}$	102.40	358.27	14.65	0.73	$1.05 \times 10^{-6}$
		$10^{-10}$	103.27	374.53	10.94	0.62	$6.28 \times 10^{-10}$
		$10^{-12}$	101.79	382.63	14.72	0.69	$2.94 \times 10^{-12}$

TABLE 4. The computational time, sparsity rate and residuals for solving anisotropic Laplace equation using spaLU.

#### REFERENCES

- [1] Amirhossein Aminfar, Sivaram Ambikasaran, and Eric Darve. A fast block low-rank dense solver with applications to finite-element matrices. *Journal of Computational Physics*, 304:170–188, 2016.
- [2] Mario Bebendorf. Efficient inversion of the galerkin matrix of general second-order elliptic operators with non-smooth coefficients. *Mathematics of computation*, 74(251):1179–1199, 2005.
- [3] Léopold Cambier, Chao Chen, Erik Boman, Sivasankaran Rajamanickam, Raymond Tuminaro, and Eric Darve. An algebraic sparsified nested dissection algorithm using low-rank approximations. *SIAM Journal on Matrix Analysis and Applications*, 41(2):715–746, 2020.
- [4] Shiv Chandrasekaran, Ming Gu, and Timothy Pals. A fast *ULV* decomposition solver for hierarchically semiseparable representations. *SIAM Journal on Matrix Analysis and Applications*, 28(3):603–622, 2006.
- [5] Hongwei Cheng, Zydrunas Gimbutas, Per-Gunnar Martinsson, and Vladimir Rokhlin. On the compression of low rank matrices. *SIAM Journal on Scientific Computing*, 26(4):1389–1404, 2005.
- [6] Timothy Davis. *Direct Methods for Sparse Linear Systems*. SIAM, 2006.
- [7] Michael Garey and David Johnson. *Computers and intractability: A guide to the theory of np-completeness*, volume 24. Society for Industrial and Applied Mathematics, 1982.
- [8] Alan George. Nested dissection of a regular finite element mesh. *SIAM journal on numerical analysis*, 10(2):345–363, 1973.
- [9] Alan George and Joseph Liu. The evolution of the minimum degree ordering algorithm. *Siam review*, 31(1):1–19, 1989.
- [10] Gene Golub and Charles Van Loan. *Matrix computations*. Johns Hopkins University Press, 4th edition, 2013.
- [11] Leslie Greengard and Vladimir Rokhlin. A fast algorithm for particle simulations. *Journal of computational physics*, 73(2):325–348, 1987.
- [12] Ming Gu and Stanley Eisenstat. Efficient algorithms for computing a strong rank-revealing qr factorization. *SIAM Journal on Scientific Computing*, 17(4):848–869, 1996.
- [13] Wolfgang Hackbusch. *Multi-grid methods and applications*. Springer Berlin Heidelberg, Berlin, Heidelberg, 1985.
- [14] Wolfgang Hackbusch. *Hierarchical Matrices: Algorithms and Analysis*, chapter Introduction, pages 3–24. Springer Berlin Heidelberg, Berlin, Heidelberg, 2015.
- [15] Wolfgang Hackbusch and Steffen Börm.  $H^2$ -matrix approximation of integral operators by interpolation. *Applied numerical mathematics*, 43(1-2):129–143, 2002.
- [16] Nathan Halko, Per-Gunnar Martinsson, and Joel Tropp. Finding structure with randomness: Probabilistic algorithms for constructing approximate matrix decompositions. *SIAM review*, 53(2):217–288, 2011.
- [17] Jun Lai, Sivaram Ambikasaran, and Leslie Greengard. A fast direct solver for high frequency scattering from a large cavity in two dimensions. *SIAM Journal on Scientific Computing*, 36(6):B887–B903, 2014.
- [18] Jun Lai, Motoki Kobayashi, and Alex Barnett. A fast and robust solver for the scattering from a layered periodic structure containing multi-particle inclusions. *Journal of Computational Physics*, 298:194 – 208, 2015.

- [19] Jun Lai and Jinrui Zhang. Fast inverse elastic scattering of multiple particles in three dimensions. *Inverse Problems*, 38(10):104002, 2022.
- [20] Richard Lipton, Donald Rose, and Robert Tarjan. Generalized nested dissection. *SIAM journal on numerical analysis*, 16(2):346–358, 1979.
- [21] Haoran Ma, Gang Bao, Jun Lai, and Junshan Lin. Inverse design of a grating metasurface for enhancing spontaneous emission through hyperbolic metamaterials. *J. Opt. Soc. Am. B*, 41(2):A79–A85, Feb 2024.
- [22] Victor Minden, Kenneth Ho, Anil Damle, and Lexing Ying. A recursive skeletonization factorization based on strong admissibility. *Multiscale Modeling & Simulation*, 15(2):768–796, 2017.
- [23] Seymour Parter. The use of linear graphs in gauss elimination. *SIAM review*, 3(2):119–130, 1961.
- [24] Vladimir Rokhlin. Rapid solution of integral equations of scattering theory in two dimensions. *Journal of Computational Physics*, 86(2):414–439, 1990.
- [25] Youcef Saad and Martin Schultz. Gmres: A generalized minimal residual algorithm for solving nonsymmetric linear systems. *SIAM Journal on Scientific and Statistical Computing*, 7(3):856–869, 1986.
- [26] Yousef Saad. *ILUT*: A dual threshold incomplete *LU* factorization. *Numerical linear algebra with applications*, 1(4):387–402, 1994.

SCHOOL OF MATHEMATICAL SCIENCES, ZHEJIANG UNIVERSITY, HANGZHOU, ZHEJIANG 310027, CHINA  
Email address: zhuxuanru@126.com

SCHOOL OF MATHEMATICAL SCIENCES, ZHEJIANG UNIVERSITY, HANGZHOU, ZHEJIANG 310027, CHINA  
Email address: laijun6@zju.edu.cn